

Supplemental Material

The early opening of the Equatorial Atlantic Gateway and the evolution of Cretaceous peak warming

Wolf Dummann, Peter Hofmann, Jens O. Herrle, Martin Frank, and Thomas Wagner

ANALYTICAL METHODS

Nd isotope analysis

Neodymium isotope analyses were performed at GEOMAR Kiel. Sea water Nd isotope signatures were leached from Fe-Mn-oxyhydroxide coatings of sediment particles, following Blaser et al. (2016).

Sediment samples were rinsed with ultrapure water and then leached for 60 min using a solution of 0.005 M hydroxylamine hydrochloride, 0.001 M Na-EDTA, and 1.5% acetic acid, buffered at pH 4. The leachate was dried and reacted with concentrated nitric acid to remove hydroxylamine hydrochloride. Rare earth elements (REE) were purified using cation exchange chromatography (0.8 mL AG50W-X12 resin, 200-400 µm mesh; Barrat et al., 1996). Neodymium was isolated from the REE fraction using Ln-spec resin (2 mL, 50-100 µm mesh; Le Fèvre and Pin, 2005). Residual organic matter in the Nd fraction was decomposed using concentrated H₂O₂.

A Nu Instruments MC-ICP-MS was used to measure the Nd isotopic composition. The ¹⁴³Nd/¹⁴⁴Nd ratios were normalized to the accepted value of the JNdi-1 standard measured repeatedly during the sample runs (¹⁴³Nd/¹⁴⁴Nd = 0.512115; Tanaka et al., 2000). The external reproducibility (2σ) was monitored using a SPEX standard solution and was between 0.26 and 0.47 εNd units. εNd was calculated from ¹⁴³Nd/¹⁴⁴Nd ratios using

$$\epsilon Nd = \left(\frac{\left(\frac{{}^{143}\text{Nd}}{{}^{144}\text{Nd}} \right)_{\text{Sample}}}{\left(\frac{{}^{143}\text{Nd}}{{}^{144}\text{Nd}} \right)_{\text{CHUR}}} - 1 \right) * 10,000 \quad (1)$$

with (¹⁴³Nd/¹⁴⁴Nd)_{CHUR}=0.512638 (Wasserburg et al., 1981). Nd isotope signatures were corrected for the in-situ decay of ¹⁴⁷Sm (εNd(t)) using an average ferromanganese crust value of ¹⁴⁷Sm/¹⁴⁴Nd=0.115 (Ling et al., 1997).

Total organic carbon and total inorganic carbon analyses

Total organic carbon (TOC) and total inorganic carbon (TIC) content was measured using a DIMATOC 100 carbon analyzer (Dimatec Corp, Germany). The carbon analyzer determines TIC content as CO₂ gas after treating the samples with phosphoric acid at 160°C. Total carbon content is analyzed by combustion of the bulk sediment at 900°C. TOC content was determined by calculating the difference between total carbon content and TIC content. Carbonate content was calculated stoichiometrically from TIC content.

Carbon isotope analysis

A new carbon isotope record of carbonate ($\delta^{13}\text{C}_{\text{carb.}}$) has been generated for DSDP 363. Carbon isotope analyses were performed at the Goethe-University Frankfurt using a Gas Bench II coupled to an MAT 253 gas source mass spectrometer using 100% H₃PO₄. A Carrara-Calcite was used as an internal standard and calibrated against NBS-18 and NBS-19. Standards reproduced within $\pm 0.02\text{‰}$ for carbon isotopes. $\delta^{13}\text{C}_{\text{carb.}}$ ratios are reported relative to the Vienna-Pee Dee belemnite standard (VPDB).

Calcareous nannofossil analysis

A total of 31 samples from DSDP Site 363 (core 26 to 40) were analyzed for calcareous nannofossils to refine the Albian biostratigraphy of Proto Decima et al. (1978). About 0.05 mg of dried sediment was placed in a plastic flask and 3 ml of water was added. The vial was placed in an ultrasonic bath for 1 minute to homogenize the suspension. The suspension was dropped on a glass slide, evenly distributed with a wooden toothpick, and dried at 60°C. A cover glass was then mounted to the glass slide with Norland Adhesive No. 61. Each sample was studied at a magnification of $\times 1250$ using a ZEISS AxioImager 2 photomicroscope. The samples were screened for about 20 minutes in random traverses to detect biostratigraphic marker species (bioevents) and important high- and low-latitude ecological marker species. Bibliographic references for the taxa under consideration can be found in Perch-Nielsen (1985), Bown et al. (1998), and Nannotax (<http://www.mikrotax.org/Nannotax3/index.html>).

RELIABILITY OF ND ISOTOPE RESULTS

Previous studies have demonstrated that leaching of dispersed Fe-Mn-oxyhydroxide reliably extracts past sea water Nd isotope signatures that are fully compatible with those obtained from coeval fish remains and foraminifera (Blaser et al., 2016; Martin et al., 2010). This is also true for sediments with complex composition and diagenesis, such as sediments

containing volcanogenic material and anoxic black shales (Martin et al., 2010). Although sea water Nd isotope signals have been successfully recovered from anoxic black shales via leaching (e.g., Dummann et al., 2020), they are unlikely to be associated with Fe-Mn oxyhydroxide coatings, which readily dissolve under reducing conditions (Martin et al., 2010). In this regard, we would like to stress that we do not make any attempt to interpret the Aptian Nd isotope signal at DSDP 364 (phase 1) in terms of water mass exchange other than claiming that local weathering inputs have dominated the Nd isotope signatures of the anoxic and isolated Kwanza Basin at the time. As discussed in a recent paper by Abbott et al. (2022), even in oxygenated waters and sediments some contributions from partial dissolution of detrital sediments or pore waters can affect both the bottom water Nd isotopic signature and the authigenic signature extracted from the sediments. This is especially true for sediments near ocean margins, which, however, is not unexpected since this is where water masses are labeled with specific dissolved Nd isotope signatures. However, even if dissolution of detrital sediments had some influence on the extracted authigenic signatures at DSDP 364, this does not call into question our conclusions concerning the opening of the Equatorial Atlantic Gateway, which are based on a marked change of 4 ϵ Nd units and the onset of more open basin conditions.

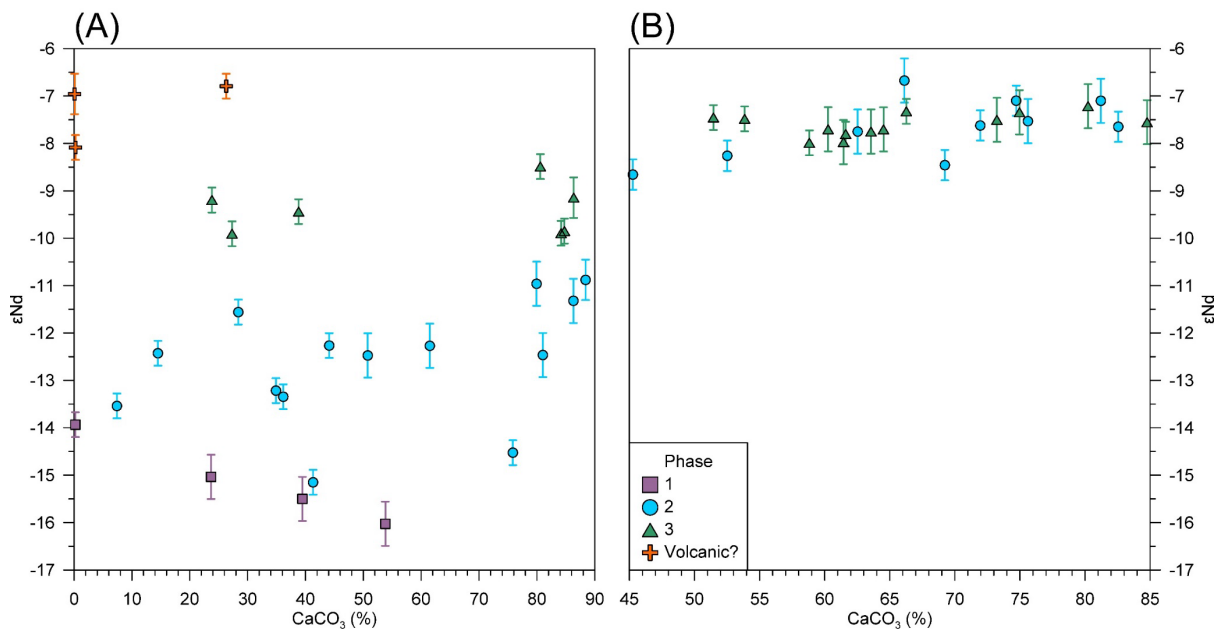


Figure S1. Cross-plots of carbonate (CaCO₃) content and sea water ϵ Nd for (A) DSDP 364 and (B) DSDP 363. Vertical error bars indicate 2SD analytical uncertainties. Key is given in (B). Phase 1, 2, and 3 refer to the time intervals of 119–113 Ma, 113–107 Ma, 107–100 Ma,

respectively. The orange crosses in (A) indicate samples deemed to reflect times of active volcanism at Walvis Ridge.

To test whether sediment composition affected the reliability of extracted sea water Nd isotope signatures, cross plots of carbonate content and ϵ_{Nd} values are provided in Supplementary Figure 1. Sea water Nd isotope signatures leached from (dolomitic) limestone samples are fully consistent with those obtained from coeval carbonate-poor shales. Samples from all three stratigraphic phases defined in our study show a similar range of CaCO_3 contents, while there are marked differences in ϵ_{Nd} between the three phases. We therefore conclude that sample mineralogy has a minor, if any, influence on the extracted sea water Nd isotope signatures.

AGE MODELS

Construction of age models

Age models for DSDP 363 and 364 were constructed assuming linear sedimentation rates between calcareous nannofossil bioevents (Supplementary Figure 2). Bioevents for DSDP 364 have been reported by Bruno et al. (2020). Bioevents for DSDP 363 are provided in Supplementary Table 1. All numerical ages are according to Gradstein et al. (2020). The veracity of the age model of DSDP 363 has been tested using carbon isotope stratigraphy. For that, we correlated our new $\delta^{13}\text{C}_{\text{carb}}$ record with the reference curve of Herrle et al. (2015). Both curves show excellent agreement in form and shape (Supplementary Figure 3). Detailed discussions on the carbon isotope stratigraphy of DSDP 364 can be found in Bruno et al. (2020) and Behrooz et al. (2018).

TABLE S1. NANNOFOSSIL BIOEVENTS AT DSDP 363

Bioevent	Depth (mbsf)*	Age (Ma) [†]
LO [§] <i>Watznaueria britannica</i>	523.37	100.30
FO [#] <i>Eiffelithus turriseiffelii</i>	542.92	103.13
FO <i>Eiffelithus monechiae</i>	612.91	107.59
FO <i>Tranolithus orionatus</i>	669.81	110.73
FO <i>Hayesites albiensis</i>	687.96	112.65
FO <i>Prediscosphaera columnata</i>	688.68	112.95
*mbsf – meters below sea floor.		
[†] Numerical ages according to Gradstein et al. (2020).		
[§] LO – last occurrence.		
[#] FO – first occurrence.		

DSDP 364

The lowermost sediment section at DSDP 364 (1032.37–1071.5 mbsf) is barren of age diagnostic fossils (Bruno et al., 2020; Kochhann et al., 2013), complicating the construction of a robust age model. We calculated numerical ages using an average sedimentation rate of $\sim 23.6 \text{ m Myr}^{-1}$ (i.e., mean sedimentation between the first occurrence of *Prediscosphaera columnata* and the last occurrence of *Watznaureria britannica* at DSDP 364) and assigning an age of $\sim 116 \text{ Ma}$ to the midpoint of the lowermost sediment section at 1084.15. We note, however, that the basal age of DSDP 364 might be slightly older. We consider the maximum age to be $\sim 119 \text{ Ma}$ (Supplementary Figure 1A), assuming that the evaporites of the Kwanza Basin, which underlie the base of DSDP 364 by a few tens of meters (Shipboard Scientific Party, 1978), are of the same age as those deposited in the Brazilian Campos, Santos, Espírito Santo basins (Sanjinés et al., 2022; Tedeschi et al., 2017). This assumption is further corroborated by a recent study that indicates a similar age for evaporites (i.e., 118.4–116.8 Ma) on the Gabon margin, north of the Kwanza Basin (Eldrett et al., 2023). The top of the lowermost section might be somewhat younger and may conformably underlie the sediments above (Supplementary Figure 2A). The minimum age is constrained by the occurrence of *P. columnata* at 1032.37 (Bruno et al., 2020), indicating an age no older than 112.95 Ma (Gradstein et al., 2020). The age of the remainder of the sediment sequence at DSDP 364 (717.23–1032.37 m) is well constrained by nannofossil biostratigraphy (Supplementary Figure 2A; Bruno et al., 2020). Numerical ages above the first occurrence of *W. britannica* have been calculated by extrapolating sedimentation rates (Supplementary Figure 2A).

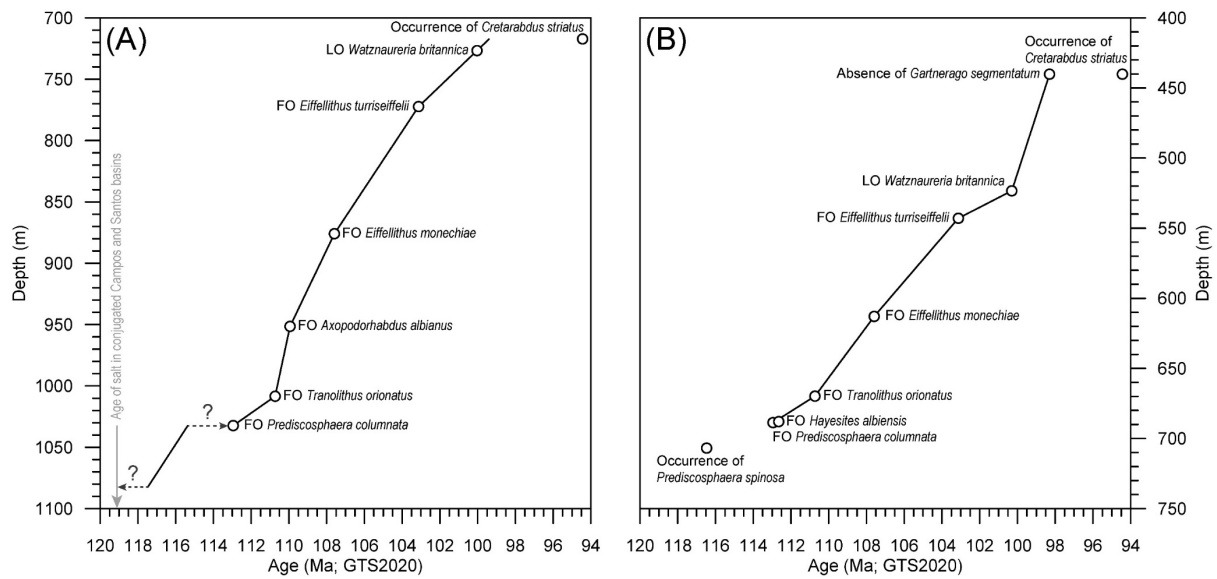


Figure S2. (A) Age-depth model for DSDP 364. Nannofossil bioevents used to construct the age model have been published in Bruno et al. (2020) (B) Age-depth model for DSDP 363. Nannofossil bioevents are provided in Supplementary Table 1. FO – First occurrence, LO – Last occurrence

DSDP 363

The succession of nannofossil bioevents observed at DSDP 363 is consistent with the biozonation of Gradstein et al. (2020). The basal age of DSDP 363 is no older than 116.47 Ma (Gradstein et al., 2020), as indicated by continuous down hole occurrence of *Prediscosphaera spinosa* (Supplementary Figure 2B). The occurrence of *Cretarhabdus striatus* up to 440.2 m indicates an age no younger than 94.44 Ma (Gradstein et al., 2020). However, we note that none of the investigated samples yielded *Gartnerago segmentatum*. We therefore assume that the top of the investigated sediment succession of DSDP 363 is older than the first occurrence of *G. segmentatum* at 98.26 Ma (Gradstein et al., 2020). This interpretation is corroborated by carbon isotope stratigraphy. We observe none of the major carbon isotope excursions that are characteristic for the Middle and Upper Cenomanian (e.g., Mid-Cenomanian Event, Oceanic Anoxic Event 2) in the $\delta^{13}\text{C}_{\text{carb}}$ record of DSDP 363 (Supplementary Figure 3). This lack of high-amplitude fluctuations supports an Early Cenomanian age for the top of the investigated succession at DSDP 363.

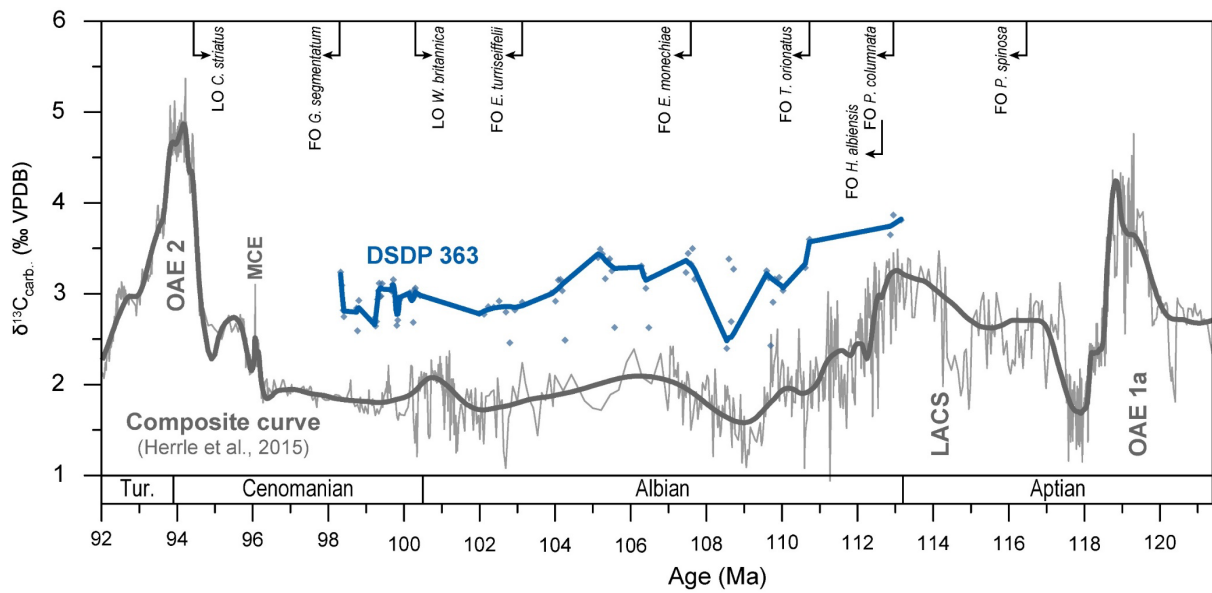


Figure S3. Carbon isotope record of carbonate ($\delta^{13}\text{C}_{\text{carb.}}$) of DSDP 363 correlated with the reference curve of Herrle et al. (2015). Characteristic carbon isotope excursions are indicated (OAE – Oceanic Anoxic Event; LACS – Late Aptian Cold Snap; MCE – Mid-Cenomanian Event). Calcareous nannofossil bioevents identified at DSDP 363 are shown on top. All trend lines are LOESS fits. Tur. – Turonian, FO – First occurrence, LO – Last occurrence

Age models of reference sites

All age models of reference sites (Figure 2) were updated to GTS2020 using the tie points reported in the original publications (see caption of Figure 2). The $\epsilon\text{Nd}(t)$ values for individual samples were then recalculated using the updated ages.

PALEOBIOGEOGRAPHY AND PROVINCIALISM

All major low latitude calcareous nannofossil bioevents of the uppermost Aptian to Lower Cenomanian have been identified at DSDP 363. The recovered calcareous nannofossils assemblage shows a typical subtropical-tropical affinity with rare to common occurrences of *Nannoconus* spp. and *Braarudosphaera* spp. and the general absence of high latitude taxa, such as *Repagulum parvidentatum*, *Sollasites falklandensis*, and *Seribiscutum primitivum*. Similar assemblages have been recovered at DSDP 364 by Bruno et al. (2020), although we find a slightly higher abundance of *Braarudosphaera* at DSDP 363. Notwithstanding these minor differences, the calcareous nannofossil assemblages at both DSDP 364 and DSDP 363 provide strong evidence for the existence of surface water connection between the North Atlantic and northern South Atlantic from at least 113 Ma onward. This interpretation is

supported by planktonic foraminiferal assemblages reported for the same stratigraphic interval at DSDP 364 (Kochhann et al., 2013).

VOLCANIC OUTGASSING OF CARBON AND CLIMATE

In addition to the time series shown in Figure 3 of the manuscript, we provide two supplementary figures to further investigate the relationship between Cretaceous climate and carbon fluxes from volcanism modeled by Müller et al. (2022). Supplementary Figure 4 shows additional paleoclimatic data sets including stacks of paleo-bottom water temperatures and paleo-subsurface temperatures based on stable oxygen isotope analyses of benthic foraminifera and belemnites, respectively (Bodin et al., 2015; Friedrich et al., 2012). Supplementary 5 shows cross-plots of reconstructed paleo-ocean temperatures and cumulative carbon outgassing at subduction zones and mid-ocean ridges, indicating overall similar carbon outgassing rates during the Late Aptian Cold Snap and the Cenomanian–Turonian thermal maximum. Consistent with the conclusions drawn in previous studies (Huber et al., 2018), this comparison suggests that volcanic outgassing of CO₂ was likely not the primary trigger of mid-Cretaceous warming.

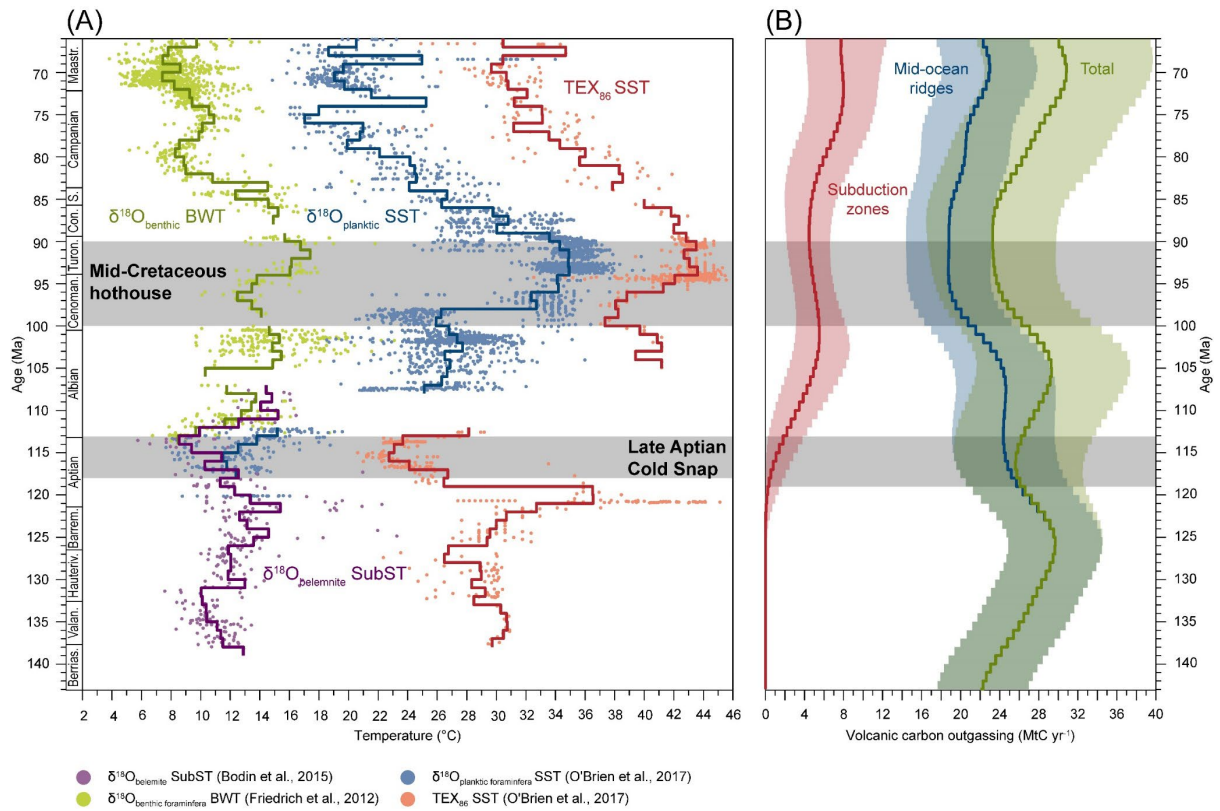


Figure S4: Comparison of Cretaceous volcanic carbon outgassing and ocean temperature evolution across the Cretaceous. (A) Ocean temperature evolution based on published proxy data compilations (Bodin et al., 2015; Friedrich et al., 2012; O'Brien et al., 2017). Sea surface temperatures (SST) in the (sub-)tropics have been reconstructed using TEX₈₆ and stable oxygen isotope records of well-preserved planktic foraminifera tests ($\delta^{18}\text{O}_{\text{planktic}}$). Early Cretaceous subsurface temperatures (SubST) and Late Cretaceous bottom water temperatures (BWT) have been reconstructed using the stable oxygen isotope composition of belemnites ($\delta^{18}\text{O}_{\text{belemnite}}$) and benthic foraminifera ($\delta^{18}\text{O}_{\text{benthic}}$), respectively. Step plots represent 1 Myr-window averages. Oxygen isotope ratios have been converted to paleo-temperatures according to Bemis et al. (1998) assuming latitudinal variations in the $\delta^{18}\text{O}$ of surface waters (Zachos et al., 1994). TEX₈₆ values were converted to sea surface temperatures using the linear calibration of O'Brien et al. (2017) and assuming a warm bias for Early Cretaceous data from the North Atlantic and South Atlantic basins (Steinig et al., 2020). (B) Carbon fluxes to the atmosphere from mid-ocean ridges and subduction zones as well as total carbon fluxes modeled by Müller et al. (2022).

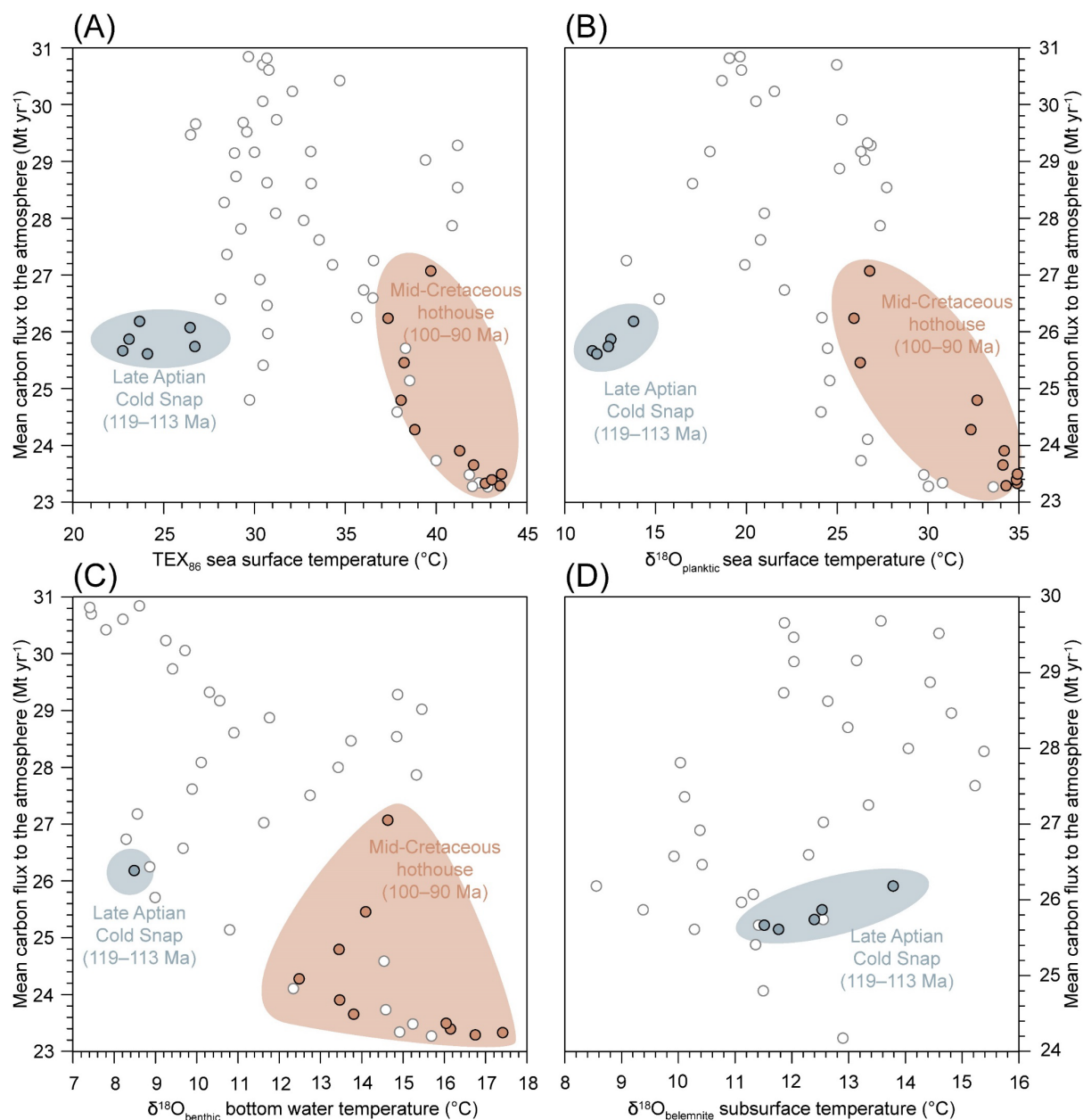


Figure S5: Correlation of ocean temperature proxy data sets (averaged over 1 Myr steps; Supplementary Figure 4A) and total volcanic carbon fluxes to the atmosphere (Müller et al., 2022) for (A) TEX₈₆ data, (B) oxygen isotope data from planktic foraminifera tests ($\delta^{18}\text{O}_{\text{planktic}}$), (C) $\delta^{18}\text{O}$ of benthic foraminifera tests ($\delta^{18}\text{O}_{\text{benthic}}$), and (D) $\delta^{18}\text{O}$ of Early Cretaceous belemnites.

SUPPLEMENTAL REFERENCES

- Abbott, A., Löhr, S., Payne, A., Kumar, H., and Du, J., 2022, Widespread lithogenic control of marine authigenic neodymium isotope records? Implications for paleoceanographic reconstructions: *Geochimica et Cosmochimica Acta*, v. 319, p. 318-336, <https://doi.org/10.1016/j.gca.2021.11.021>.
- Barrat, J. A., Keller, F., Amossé, J., Taylor, R. N., Nesbitt, R. W., and Hirata, T., 1996, Determination of rare earth elements in sixteen silicate reference samples by ICP-MS after Tm addition and ion exchange separation: *Geostandards Newsletter*, v. 20, p. 133-139, <https://doi.org/10.1111/j.1751-908X.1996.tb00177.x>.
- Bemis, B. E., Spero, H. J., Bijma, J., and Lea, D. W., 1998, Reevaluation of the oxygen isotopic composition of planktonic foraminifera: Experimental results and revised paleotemperature equations: *Paleoceanography*, v. 13, p. 150-160, <https://doi.org/10.1029/98PA00070>.
- Bodin, S., Meissner, P., Janssen, N. M. M., Steuber, T., and Mutterlose, J., 2015, Large igneous provinces and organic carbon burial: Controls on global temperature and continental weathering during the Early Cretaceous: *Global and Planetary Change*, v. 133, p. 238-253, <https://doi.org/10.1016/j.gloplacha.2015.09.001>.
- Bown, P., 1998, *Calcareous nannofossil biostratigraphy*: London, Chapman&Hall, 314 p.
- Eldrett, J. S., Bergman, S. C., Heine, C., Edwards, P., Jakeman, M., Miles, N., Hambach, B., Bohaty, S. M., and Wilding, M. R., 2023, Integrated bio-and chemo-stratigraphy for Early Cretaceous strata offshore Gabon: Additional constraints on the timing of salt deposition and rifting of the South Atlantic: *Marine and Petroleum Geology*, v. 148, 106037, <https://doi.org/10.1016/j.marpetgeo.2022.106037>.
- Herrle, J. O., Schröder-Adams, C. J., Davis, W., Pugh, A. T., Galloway, J. M., and Fath, J., 2015, Mid-Cretaceous High Arctic stratigraphy, climate, and oceanic anoxic events: *Geology*, v. 43, p. 403–406, <https://doi.org/10.1130/G36439.1>.
- Huber, B. T., MacLeod, K. G., Watkins, D. K., and Coffin, M. F., 2018, The rise and fall of the Cretaceous Hot Greenhouse climate: *Global and Planetary Change*, v. 167, p. 1-23, <https://doi.org/10.1016/j.gloplacha.2018.04.004>.
- Le Fèvre, B., and Pin, C., 2005, A straightforward separation scheme for concomitant Lu–Hf and Sm–Nd isotope ratio and isotope dilution analysis: *Analytica Chimica Acta*, v. 543, p. 209–221, <https://doi.org/10.1016/j.aca.2005.04.044>.
- Ling, H. F., Burton, K. W., O'Nions, R. K., Kamber, B. S., Von Blanckenburg, F., Gibb, A. J., and Hein, J. R., 1997, Evolution of Nd and Pb isotopes in Central Pacific seawater from ferromanganese crusts: *Earth and Planetary Science Letters*, v. 146, p. 1–12, [https://doi.org/10.1016/S0012-821X\(96\)00224-5](https://doi.org/10.1016/S0012-821X(96)00224-5).
- Perch-Nielsen, K., 1985, Mesozoic calcareous nannofossils, *in* Bolli, H., Saunders, J., and Perch-Nielsen, K., eds., *Plankton stratigraphy*: Cambridge, Cambridge University Press, p. 329–426.

- Proto Decima, F., Medizza, F., and Todesco, L., 1978, Southeastern Atlantic Leg 40 calcareous nannofossils, *in* Bolli, H. M., and Ryan, W. B. F., et al., eds., Initial Reports of the Deep Sea Drilling Project, Volume 40: Washington, D.C., U.S. Government Printing Office, p. 571–634, <https://doi.org/10.2973/dsdp.proc.40.112.1978>.
- Shipboard Scientific Party, 1978, Angola Continental Margin—Sites 364 and 365, *in* Bolli, H. M., and Ryan, W. B. F., et al., eds., Initial Reports of the Deep Sea Drilling Project, Volume 40: Washington, D.C., U.S. Government Printing Office, p. 357–455, <https://doi.org/10.2973/dsdp.proc.40.104.1978>.
- Steinig, S., Dummann, W., Park, W., Latif, M., Kusch, S., Hofmann, P., and Flögel, S., 2020, Evidence for a regional warm bias in the Early Cretaceous TEX₈₆ record: Earth and Planetary Science Letters, v. 539, 116184, <https://doi.org/10.1016/j.epsl.2020.116184>.
- Tanaka, T., Togashi, S., Kamioka, H., Amakawa, H., Kagami, H., Hamamoto, T., Yuhara, M., Orihashi, Y., Yoneda, S., and Shimizu, H., 2000, JNdi-1: a neodymium isotopic reference in consistency with LaJolla neodymium: Chemical Geology, v. 168, p. 279–281, [https://doi.org/10.1016/S0009-2541\(00\)00198-4](https://doi.org/10.1016/S0009-2541(00)00198-4).
- Wasserburg, G. J., Jacobsen, S. B., DePaolo, D. J., McCulloch, M. T., and Wen, T., 1981, Precise determination of Sm/Nd ratios, Sm and Nd isotopic abundances in standard solutions: Geochimica et Cosmochimica Acta, v. 45, p. 2311–2323, [https://doi.org/10.1016/0016-7037\(81\)90085-5](https://doi.org/10.1016/0016-7037(81)90085-5).
- Zachos, J. C., Stott, L. D., and Lohmann, K. C., 1994, Evolution of Early Cenozoic marine temperatures: Paleoceanography, v. 9, p. 353–387, <https://doi.org/10.1029/93PA03266>.